Analysis of the podocyte cytoskeleton on CYTOO micropatterns using the Operetta high-content analysis system.

Key features

- Nephrotoxicity screening on the Operetta® system
- Cell normalization on CYTOO micropatterns
- Visualization of compound effects through calculation of an average cell

Background

Drug-induced nephrotoxicity is one of the most common reasons for the failure of new chemical entities in clinical trials during drug development. It is also a serious problem for approved drugs such as contrast media [Deray, 2006] or the widely-used non-steroidal anti-inflammatory drugs (NSAIDs) [Clive and Stoff, 1984]. The mechanisms of drug-induced nephrotoxicity differ between individual drugs or drug classes [Nolin and Himmelfarb, 2010], but it is now widely accepted that the podocyte is one of the key cell types affected by nephrotoxicity or renal injury. This is also true for a variety of kidney diseases ranging from rare congenital kidney disorders to frequently observed diabetic nephropathy [Mathieson, 2012].

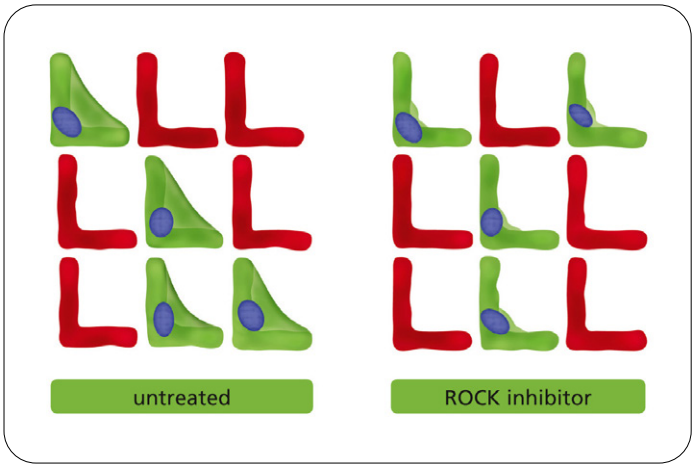

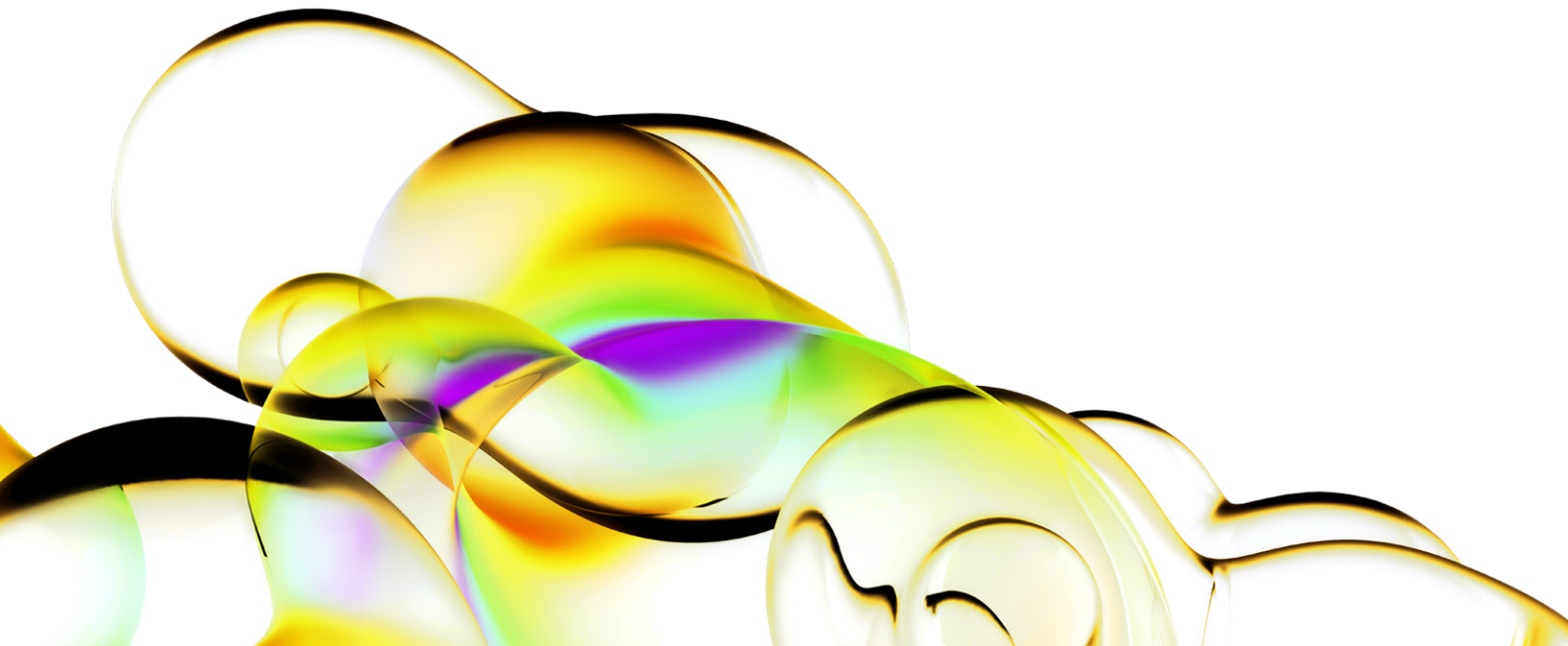

The podocyte is a highly differentiated epithelial cell type with a unique cytoskeletal architecture. These cells are found on the outside of the glomerulus and play a key role in the formation of the glomerular filtration barrier within the Bowman's capsule. The high degree of cytoskeletal organization is maintained via the complex interplay of microtubules, intermediate filaments and the actin cytoskeleton, which allow the formation of small foot processes of the podocyte. These foot processes are small cellular protrusions that exist in their thousands in each podocyte and that form a complex mesh interconnected by the slit diaphragm on the outside of the glomerulus (Figure 1). The cytoskeleton of the podocytes is subject to dynamic regulation with constant changes in contractility and motility [Welsh and Saleem, 2012]. The complex cytoskeleton and the slit diaphragm are particularly targeted and disrupted during kidney injury and disease [Wang et al., 2012].

Here we present a high content screening application in collaboration with Evotec AG, to analyze the integrity of the podocyte actin cytoskeleton. Using the Operetta high-content analysis system we acquired images of podocytes grown on CYTOOchips™ and analyzed drug-induced changes in podocyte morphology using the Harmony® high content imaging and analysis software.

Application

Conditionally immortalized human podocytes were cultured as described in Saleem et al., 2002. Cells were differentiated in RPMI-1640 containing 2% FCS for 10-14 days. Cells were seeded at a density of 80,000 cells per well onto CYTOOchips™ contained within a standard 6-well cell culture plate. The L-shaped micropatterns on the CYTOOchips™ had an area of 1600 μm^2 and were coated with Red Fluorescent Fibronectin (FN650) (CYTOOchips™ 20x20 L-L-FN650; Cat. No. 10-015-13-06). Cells of two different chips were either left untreated (control) or were treated with 10 µM ROCK Inhibitor Y-27632 (Sigma) for 1 hr prior to fixation with 4% paraformaldehyde. Cells were permeabilized with saponin and stained with Alexa Fluor® 488 Phalloidin (1:50 dilution) and Hoechst (2 ng/mL). Stained CYTOOchips™ were mounted onto microscope slides using Fluoromount-G™ (Beckman Coulter E2511-R901).

Using an Operetta system equipped with a slide holder and a 10X high NA objective, we acquired widefield images of the three channels representing the micropatterns, the actin cytoskeleton and the nuclei (Figure 2). We measured 54 image fields for both the treated and untreated CYTOOchips™.

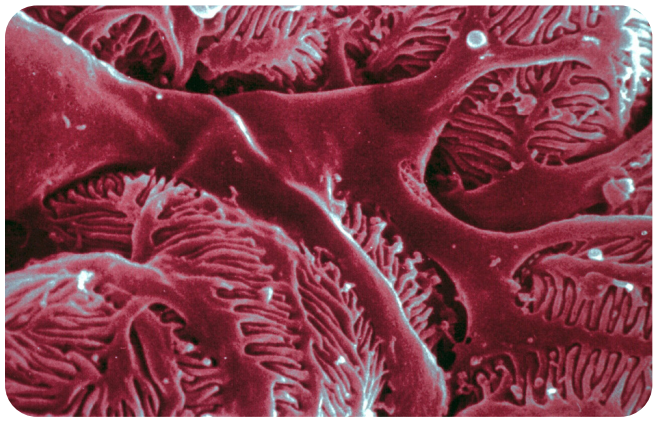

Figure 1: Colored Scanning Electron Micrograph (SEM) of podocyte cells on a glomerulus in the kidney. The podocytes' foot processes form a complex mesh covering the blood capillaries in the glomerulus.

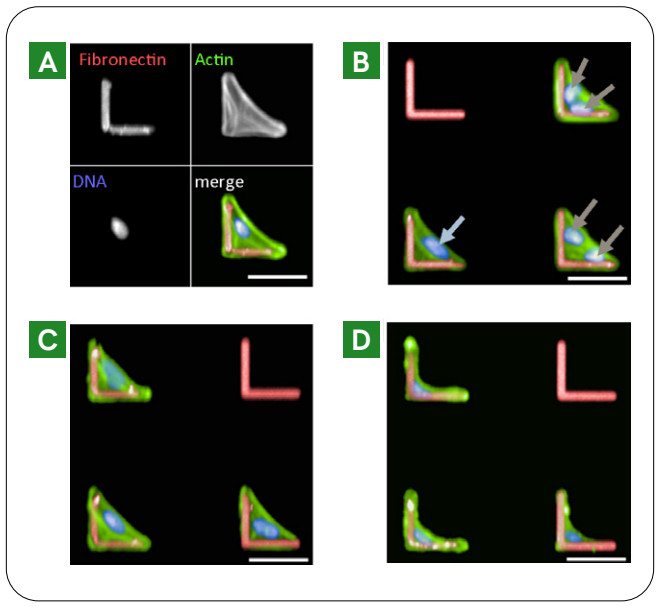

Figure 2: Podocytes grown on CYTOO micropatterns.
A) Micrographs of a single podocyte grown on an L-shaped micropattern. B) Approximately 50% of the micropatterns were occupied by podocytes and, based on the nuclear staining; approximately 50% of these were occupied by more than one cell (dark grey arrows). For the analysis, we focused on isolated podocytes on micropatterns (light blue arrow). C) Untreated podocytes form a stress fiber between both arms of the micropattern and adopt a triangular shape. D) Podocytes treated with a ROCK inhibitor adopt an L-shape.

Analysis of micropattern occupation by podocytes

We made two initial observations from studying the images. Firstly, only around half of the micropatterns were occupied by podocytes and, among these, a significant fraction was occupied by two or more cells at once (Figure 2B). Secondly, the shape of treated podocytes clearly differed from the shape of untreated cells. Healthy podocytes adopted a triangular morphology with a pronounced stress fiber between both arms of the L-shaped micropattern (Figure 2C). In contrast, the treated podocytes seemed to be unable to form such a stress fiber and therefore adopted an L-shape (Figure 2D).

One of the advantages of the CYTOO micropattern technology is that the cell-to-cell variation is very low. To exploit this benefit we had to ensure that only micropatterns that were occupied by a single podocyte were considered. Therefore, we conducted these subsequent image analysis steps: a) segment micropatterns, b) select occupied micropatterns and c) select micropatterns with a single podocyte (mono-occupied micropatterns).

As a first step, we segmented the individual micropatterns using the *Find Nuclei* building block of the Harmony software tuned with an atypical set of parameters. Similar to nuclei, the segmented micropatterns acted as the starting point for further image analysis. Next, we segmented the cytoplasm of podocytes growing on micropatterns using the *Find Cytoplasm* building block on the actin channel image. This step did not discriminate between whether there was only one or several podocytes growing on a micropattern, and the entire actin cytoskeleton was segmented as a single cell. Thus, objects that were identified in this way could contain more than one nucleus. Empty micropatterns were now removed from the analysis using the *Select Population* building block, with the absence of AlexaFluor® 488 staining as the selection criterion.

To separate mono- from poly-occupied micropatterns, we used Harmony software's STAR morphology analysis, which analyzes the fluorescence distribution of a given channel within each object. The fluorescence distribution can be analyzed with respect to **S**ymmetry, **T**hreshold Compactness, **A**xial, **R**adial and Profile properties (STAR). The distribution of the Hoechst staining within the identified object differs markedly between a single nucleus and multiple nuclei per object. Using the calculated STAR morphology properties, we trained Harmony software's supervised machine-learning module, PhenoLOGIC™, to distinguish between mono- and poly-occupied micropatterns. PhenoLOGIC autonomously selected more than 10 properties and calculated the linear combination with the best discriminative power for the phenotypic classes.

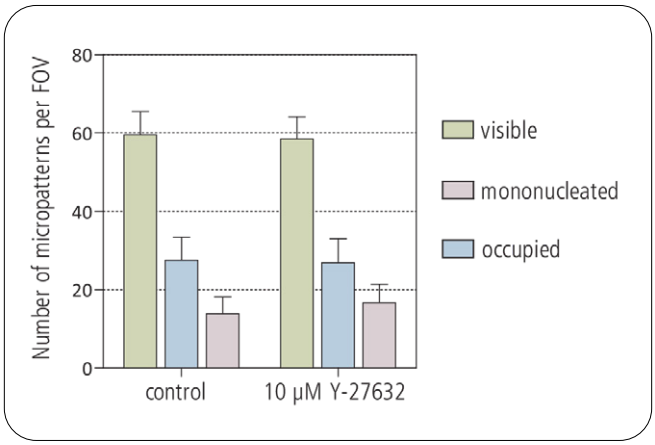

Figure 3: Quantification of micropattern occupation per field of view (FOV). Error bars indicate standard deviation (n=54 image fields). Per FOV there were 59.5 ± 1.6 and 58.5 ± 1.5 fully visible micropatterns for the control and the inhibitor-treated CYTOOchip™, respectively. We found 27.5 ± 1.6 micro-patterns occupied per FOV on the control chip and 26.9 ± 1.7 occupied in the treated sample. Of those, only 13.9 ± 1.2 micropatterns in the control sample and 16.6 ± 1.3 in the treated sample were occupied by only one single cell.

Per field of view (FOV), almost 60 micropatterns were fully visible and we found that approximately 50% of the micropatterns were occupied by one or more podocytes. Among the occupied micropatterns, about 50% were occupied by only one single cell. In summary, only 23.4% and 28.4% of the visible micropatterns in the control and the treated sample, respectively, were considered valid and were used for further analysis (Figure 3).

Quantifying podocyte morphology

To quantify changes in the actin cytoskeleton of the podocytes upon treatment with ROCK inhibitor, we calculated intensity properties (sum, mean, median, standard deviation) and morphological properties (roundness, area) of the actin channel. Since we used the CYTOOchips™ we could not analyze different wells per sample. Therefore, we considered the chip as one well and analyzed the single cell data (Figure 4).

In addition to analyzing the morphological changes, we also analyzed the assay statistics. Essentially, we wanted to answer the question of how many valid micropatterns (i.e. podocytes) we need to measure in order to obtain a reasonable Z′ factor. This was of particular interest for two reasons:

1) We observed only the two extreme phenotypes (L-shaped or triangular) and no intermediate phenotypes.

2) We found a significant number of L-shaped cells in the untreated condition, and triangular cells in the ROCK inhibitor-treated condition. Therefore, if sampling just a small total cell number, cells of the wrong phenotype would have a strong impact on the calculated mean morphology.

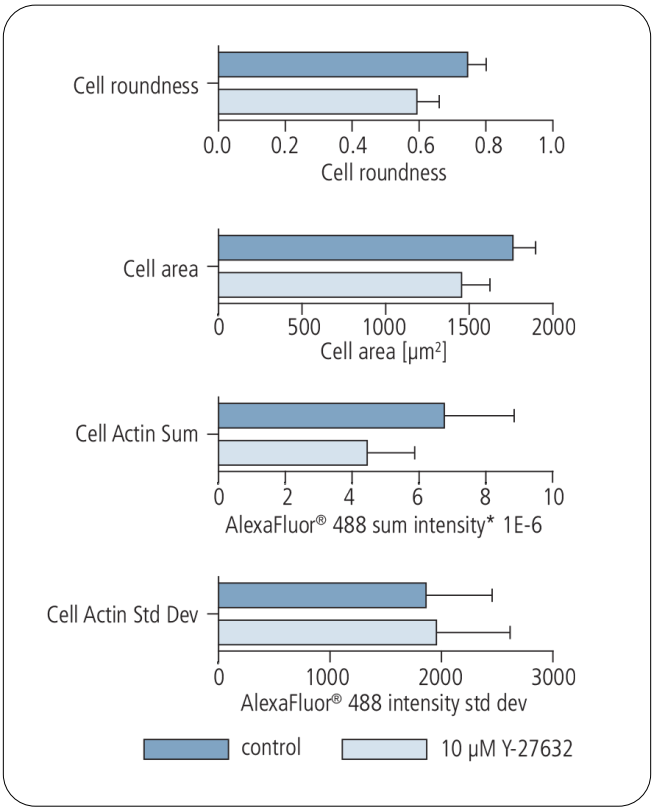

Figure 4: Morphology and intensity properties describing the actin cytoskeleton of untreated (control) vs. ROCK inhibitor (Y-27632) treated podocytes. Cell roundness is the greatest difference between the two samples whereas there is no significant difference in the standard deviation (StdDev) of the actin staining. Error bars indicate standard deviation (n=749 cells (control) and n=898 cells (Y-27632)).

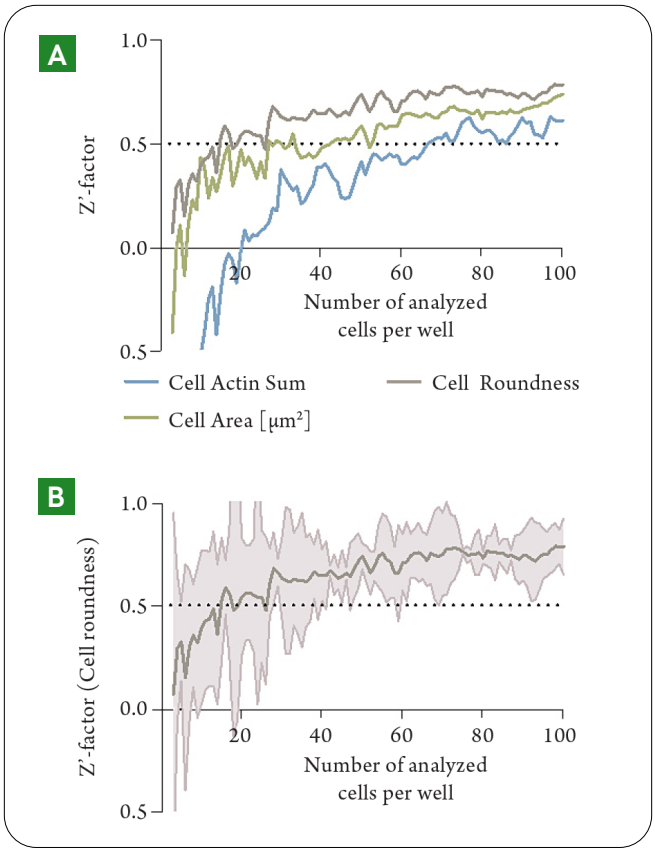

Figure 5: Statistical analysis of assay quality using the Z′ factor as a function of the contributing cells per well. A) Comparison of the 3 best obtained readouts. As expected, the Z′ factor increases with the number of contributing cells. B) Z′ factor of the property Cell Roundness plotted against the number of analyzed cells per well. The grey area indicates the 95% confidence interval. The variation in the Z′ factor decreases with an increasing number of analyzed cells since the sampled cells more reliably reflect the real distribution of triangular and L-shaped podocytes.

To perform this analysis we exported single cell results from the Harmony software and randomly grouped these single cells into virtual wells using a VBA script run in Microsoft® Excel®. In short, we clustered N cells of the positive and negative control into 3 wells and calculated the Z′ factor over these wells for each property. To average out fluctuations in the Z′ score, we performed this clustering 5 times and plotted the mean Z′ factor versus the number of cells per virtual well (Figure 5).

Not surprisingly, the mean Z′ factor increases as the number of cells that contribute to the calculation of the value increases. Among the calculated properties that describe the podocyte's actin cytoskeleton, the cell roundness yielded the best Z′ factor, followed by the cell area and the sum intensity of the Alexa Fluor® 488 Phalloidin staining (Figure 5A). We also studied the variation of the mean Z′ factor for the property cell roundness and found that the width of the 95% confidence interval decreases with increasing cell number (Figure 5). This observation can be easily explained with the more representative sample dataset. Outliers (triangular in the ROCK-treated condition and L-shaped in the control situation) do not seriously influence the Z′ factor when they are part of a bigger sample set. An excellent Z′ factor of above 0.5 can be reliably reached if more than 40 cells per well and treatment condition are imaged and the property cell roundness is used as the readout.

Calculating an average cell using acapella software

CYTOO suggests Reference Cell™ as a tool to easily visualize phenotypic changes between different treatment conditions. We followed a similar approach but used the Acapella® high content imaging and analysis software. In brief, micropatterns that were occupied by a single podocyte were excised from the original image in a 100 x 100 px bounding box. These images were superimposed based on the red fluorescent micropattern and a color-coded rainbow intensity was used to highlight the main sites of the actin intensity distribution (Figure 6A). In this way, an interference image from more than 650 cells was obtained, which accentuates the predominant localization of the actin staining for each phenotype. The biggest difference between the control and the Y-27632-treated cells is the absence of the pronounced stress fiber between both arms of the L-shaped micropattern (Figure 6B).

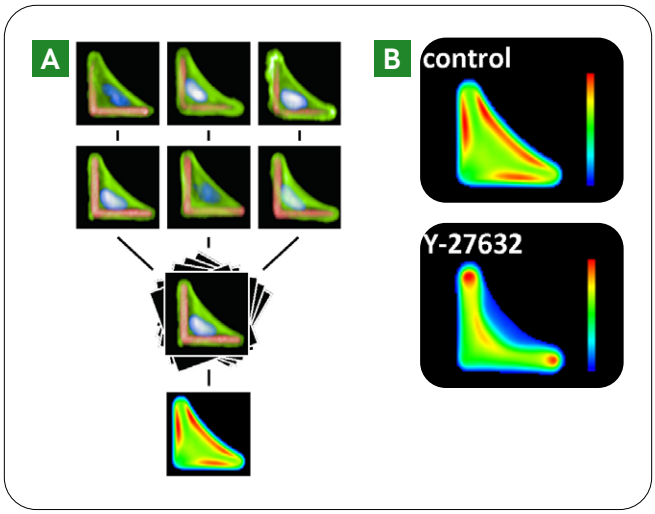

Figure 6: Calculation of an average cell for each treatment phenotype. A) Individual micropatterns were excised from the original images. The obtained cell images were then superimposed based on the red fluorescent micropatterns. B) False-color images of the average cells for both phenotypes obtained from 665 control cells and 705 Y-27632-treated cells. The average intensity of the actin staining is reflected in the color code from red (strong signal) to blue (weak signal).

Conclusion

In this study we have shown how CYTOO micropatterns can be applied to establish a new high content screening system for nephrotoxicity. The chosen approach may seem artificial, but podocytes growing on micropatterns are challenged to form complex cytoskeletal structures similar to the *in vivo* situation in the glomerular filtration barrier. Although pronounced actin stress fibers are a key feature of podocytes grown on standard cell culture surfaces, a large degree of cell to cell variability makes analysis of actin fiber re-arrangement problematic (personal communication, Evotec AG). As a consequence, alterations in the podocytes that impair their capability to react to cytoskeletal stress are more difficult to detect in standard cell culture models.

By applying the easy-to-use, yet powerful, building blocks of the Harmony software, we identified micropatterns occupied by a single podocyte and calculated properties which describe the podocyte morphology and actin intensity properties. The analysis of single cell data provided by the Harmony software revealed that at least 40 cells per well should be analyzed to robustly obtain an excellent Z′ factor which discriminates between the two treatments. Due to the large FOV of the Operetta system, only 3 fields need to be acquired for a reliable analysis.

In order to obtain a visual representation of the morphological changes in the podocytes, we generated an aligned overlay image of more than 650 cells in each treatment condition using the Acapella software. The resulting average cell is similar to the Reference Cell™ that has been proposed by CYTOO and can be used to compare different treatment conditions visually. In addition, the average cell allows for the compilation of different marker stains into one image, even though the marker proteins were not labeled in the same cells.

In summary, the flexible acquisition of images on the Operetta system and the building block-based analysis of the Harmony software provided ideal tools to establish a nephrotoxicity screening system using podocytes cultivated on CYTOO micropatterns.

References

1. Clive, D.M. and Stoff, J.S. (1984): Renal syndromes associated with nonsteroidal antiinflammatory drugs. *The New England Journal of Medicine*, 310 (9), 563–72.
2. Deray, G. (2006): Dialysis and iodinated contrast media. *Kidney International. Supplement*, (100), S25–9.
3. Mathieson, P.W. (2012): The podocyte as a target for therapies – new and old. *Nature Reviews Nephrology*, 8 (1), 52–6.
4. Nolin, T.D. and Himmelfarb, J. (2010): Mechanisms of drug-induced nephrotoxicity. *Handbook of Experimental Pharmacology*, (196), 111–30.
5. Saleem, M.A., O'Hare, M.J., Reiser, J., Coward, R.J., Inward, C.D., Farren, T., Xing, C.Y., Ni, L., Mathieson, P.W. and Mundel, P. (2002): A conditionally immortalized human podocyte cell line demonstrating nephrin and podocin expression. *Journal of the American Society of Nephrology*, 13 (3), 630–8.
6. Wang, L., Ellis, M.J., Gomez, J.A., Eisner, W., Fennell, W., Howell, D.N., Ruiz, P., Fields, T.A. and Spurney, R.F. (2012): Mechanisms of the proteinuria induced by Rho GTPases. *Kidney International*, 81 (11), 1075–85.
7. Welsh, G.I. and Saleem, M.A. (2012): The podocyte cytoskeleton – key to a functioning glomerulus in health and disease. *Nature Reviews Nephrology*, 8 (1), 14–21.

External image

Figure 1, Colored Scanning Electron Micrograph (SEM) of podocyte cells on a glomerulus in the kidney:
© www.visualphotos.com (CMEABG-UCBL/Phanie)

Authors

Matthias Fassler
Olaf Deppe
Karin Boettcher

Revvity, Inc.

Kenneth Young
Stefan Jaeger

Evotec AG